Inorganic Chemistry
Article
Cite This: Inorg. Chem. 2018, 57, 4510−4515
pubs.acs.org/IC

Selective Photo-Induced Oxidation with O_2 of a Non-Heme Iron(III) Complex to a Bis(imine-pyridyl)iron(II) Complex

Juan Chen,[†] Duenpen Unjaroen,[†] Stepan Stepanovic,[‡] Annie van Dam,[§] Maja Gruden,*[,‡] and Wesley R. Browne*[,†]

[†]Stratingh Institute for Chemistry, Faculty of Science and Engineering, University of Groningen, Nijenborgh 4, 9747AG Groningen, The Netherlands

[‡]University of Belgrade, Faculty of Chemistry, Studentski trg 12−16, 11000 Belgrade, Serbia

[§]Interfaculty Mass Spectrometry Center, University of Groningen, Groningen, The Netherlands

Supporting Information

ABSTRACT: Non-heme iron(II) complexes of pentadentate N4Py (*N,N*-bis(2-pyridylmethyl)-*N*-bis(2-pyridyl)methylamine) type ligands undergo visible light-driven oxidation to their iron(III) state in the presence of O_2 without ligand degradation. Under mildly basic conditions, however, highly selective base catalyzed ligand degradation with O_2, to form a well-defined pyridyl-imine iron(II) complex and an iron(III) picolinate complex, is accelerated photochemically. Specifically, a pyridyl-CH_2 moiety is lost from the ligand, yielding a potentially N4 coordinating ligand containing an imine motif. The involvement of reactive oxygen species other than O_2 is excluded; instead, deprotonation at the benzylic positions to generate an amine radical is proposed as the rate determining step. The selective nature of the transformation holds implications for efforts to increase catalyst robustness through ligand design.

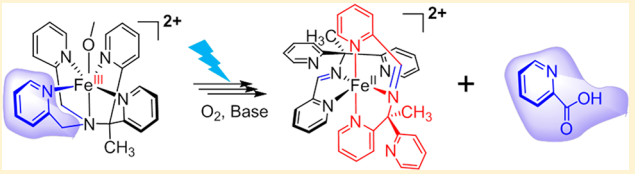

INTRODUCTION

The switch to catalysis employing sustainable and abundant metals, in particular first row transition metals, such as manganese, copper, and iron, continues to be a major challenge. Non-heme iron complexes have received substantial attention in the catalyzed oxidation of organic substrates, in particular those complexes based on the pyridyl-alkylamine type ligands that are inspired by structural and mechanistic studies of the active sites of metallo-enzymes.[1] Typical examples of such ligands are the amine-based N4 and N5 ligands (e.g., TMC, 1,4,8,11-tetramethyl-1,4,8,11-tetraazacyclotetradecane;[2] TPA, tris(2-pyridylmethyl)amine;[3] and N4Py, *N,N*-bis(2-pyridylmethyl)-*N*-bis(2-pyridyl)methylamine,[4] as well as their derivatives) which have been used to isolate especially iron(IV) oxido species and establish their relevance in oxidation catalysis.[3−8] For many of these catalysts, deactivation due to ligand degradation is a major challenge to their broader application.[9−11] The presence of reactive oxidation species is intrinsic to oxidation reactions. Hence, building more robust catalyst systems requires intimate knowledge of ligand degradation mechanisms. Furthermore, the rapidly increasing interest in photocatalytic reactions, e.g., with iron complexes,[12,13] adds an extra dimension to understanding ligand degradation and catalyst deactivation.

Recently we reported the photochemistry of a group of complexes based on pentadentate ligands (e.g., N4py and MeN4py (L)), in their Fe(II),[16] Fe(III), and Fe(IV) oxidation states (Scheme 1).[14] Visible irradiation of **1a** {Fe(II)L(OCH_3)} in air-equilibrated methanol results in its oxidation to **1** (Fe(III)L(OCH_3), Scheme 1b), which could be reversed quantitatively by electrochemical or chemical reduction. More recently we demonstrated that the Fe(IV)=O and Fe(III)−O−Fe(III) complexes of MeN4Py and N4py undergo reduction to $[(MeN4Py)Fe^{III}(OCH_3)]^{2+}$ (**1**) and $[(MeN4Py)Fe^{II}(OCH_3)]^{+}$ (**1a**), respectively, upon near-UV irradiation in the absence of oxygen (with concomitant oxidation of methanol to methanal, Scheme 1a). In these studies, although the photo-induced oxidations and reductions proceeded without ligand degradation, it was noted that irreversible changes occurred under extended irradiation (several hours), in the presence of O_2, to yield an unassigned species.

Here we show under basic conditions an additional light induced pathway (Scheme 1c) that leads to selective oxidative ligand degradation that occurs in the presence of O_2 and a base. Specifically, a pyridyl-CH_2 moiety is lost from the MeN4Py ligand, yielding a potentially N4 coordinating ligand containing an imine motif. The degraded ligand then coordinates to the Fe(II) ion in a 2:1 manner to form $\mathbf{A}^{2+}$. The remaining iron ions form Fe(III) complexes of picolinate. $\mathbf{A}^{2+}$ is photochemically inert, and its formation is shown to be driven by an initial deprotonation followed by reaction with O_2 rather than C−H oxidation by an Fe(IV)=O intermediate or other reactive oxygen species. The mechanism for the formation of the photoproduct is explored, and the implications this light-driven

Received: January 24, 2018
Published: March 30, 2018

DOI: 10.1021/acs.inorgchem.8b00187
Inorg. Chem. 2018, 57, 4510−4515

Scheme 1. (a) Light-Driven Reduction of Fe(IV)=O[14] and Fe(III)−O−Fe(III) with Methanol Oxidation,[15] (b) Light-Driven Oxidation of Fe(II) Complexes with O_2,[16] and (c) the Light Induced Oxidative Selective Ligand Degradation Described in This Work

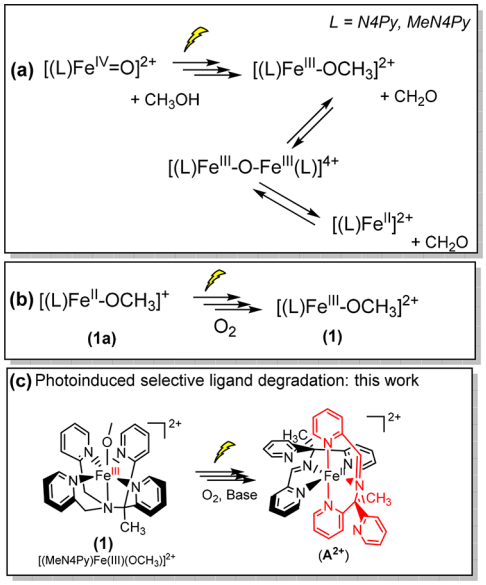

reaction holds for ligand design strategies to avoid ligand breakdown in oxidation catalysis are discussed.

The selectivity observed in the case of the MeN4Py complex contrasts with that observed for the corresponding N4Py complex, which forms an ill-defined mixture of species. The highly selective nature of the conversion of **1** to $\mathbf{A}^{2+}$, in the case of the MeN4Py complex, allows for quantitative conversion to a complex bearing two singly oxidized MeN4Py ligands, which were isolated and characterized by UV−vis absorption, (resonance) Raman spectroscopy, FTIR and variable temperature ^{1}H NMR spectroscopy, ESI-MS analysis, cyclic voltammetry, and UV−vis absorption spectroelectrochemistry. ^{1}H NMR spectral and DFT data reveal that $\mathbf{A}^{2+}$ is a mixture of several relatively rapidly interconverting isomers of the complex.

RESULTS AND DISCUSSION

The UV−vis absorption spectrum of **1** in methanol with Et_3N or NaOAc shows the appearance of new bands at 575 nm over time (i.e., 10 h, Figure S1 in the Supporting Information). Irradiation (λ_{exc} = 365 nm) accelerates (<5 min) the appearance of the 575 nm band, as well as bands at 380 and 492 nm, dramatically (Figure 1). Similar changes are observed with NaOAc instead of Et_3N (Figure S2). The wavelength dependence of the rate of formation of $\mathbf{A}^{2+}$ corresponds to the absorbance with irradiation at 300, 405, and 457 nm showing rapid conversion. Irradiation at 590 nm results in an increase in absorbance at 575 nm at a much slower rate but, nevertheless, a rate greater than that observed for the thermal reaction alone (Figure S3).

The presence of a base and O_2 is sufficient for achieving the conversion of **1** to $\mathbf{A}^{2+}$, albeit over several hours (Figure S1), indicating that light accelerates an otherwise thermal reaction. In the absence of added base (i.e., Et_3N, NaOAc, etc.), the formation of $\mathbf{A}^{2+}$ is not significant. Furthermore, irradiation of **1** in deoxygenated methanol results in its photoreduction to $[(MeN4Py)Fe^{II}OCH_3]^{2+}$ (**1a**) only, even in the presence of a base (Figures 2 and S4) (eq 1b), confirming that O_2 is essential

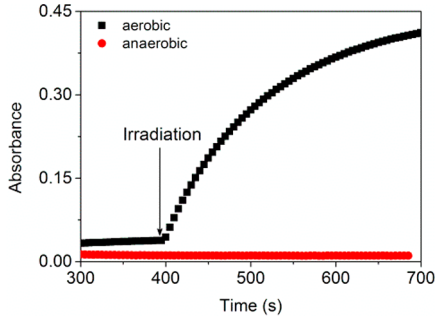

Figure 2. Absorbance at 575 nm of **1** in argon-purged (red) and air-equilibrated methanol over time. Irradiation was initiated 400 s after addition of 50 equiv of Et_3N. See Figures 1 and S4 for full spectra.

to the formation of $\mathbf{A}^{2+}$. In the presence of a base and O_2, reduction to **1a** competes with the formation of $\mathbf{A}^{2+}$ (eqs 1a and 1b) and the product ratio (**1a** vs $\mathbf{A}^{2+}$) is dependent on the time delay between addition of the base and commencement of irradiation (Figure S5).

$$\mathbf{1} \xrightarrow[\text{methanol}]{h\nu,\ \text{base},\ O_2} \mathbf{A}^{2+} \qquad \text{equation 1a}$$

$$\mathbf{1} \xrightarrow[\text{methanol}]{h\nu,\ \text{base},} \mathbf{1a} \qquad \text{equation 1b}$$

Indeed, almost full conversion from **1** to $\mathbf{A}^{2+}$ was observed when irradiation was commenced 3−5 min after addition of the base to **1** in methanol, with a quantum yield at 365 nm of ca. 0.14 (see Supporting Information), whereas if irradiation is

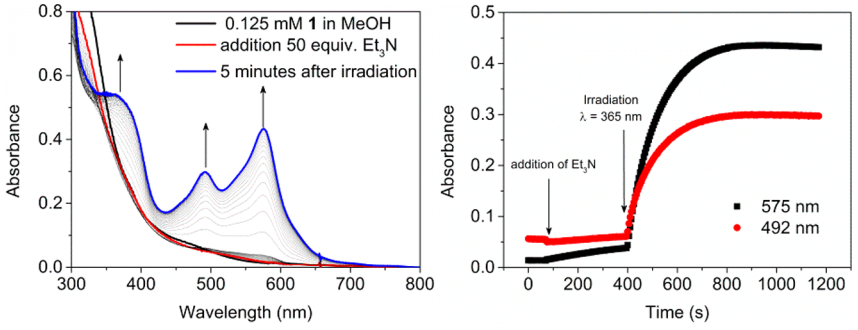

Figure 1. (Left) UV−vis absorption spectra of **1** (0.125 mM) (black) in methanol under irradiation at 365 nm with 50 equiv of Et_3N. (Right) Absorbance at 492 and 575 nm; Et_3N was added at 75 s, and irradiation was initiated at 400 s.

DOI: 10.1021/acs.inorgchem.8b00187
Inorg. Chem. 2018, 57, 4510−4515

commenced immediately after addition of the base, a mixture of $\mathbf{A}^{2+}$ and **1a** is obtained. Furthermore, whereas[5] addition of excess (50 equiv) H_2O_2 to **1** and anaerobic photoproduct **1a** leads to the immediate formation of an Fe(III)-OOH species, addition of H_2O_2 to $\mathbf{A}^{2+}$ has no effect on its absorption spectrum (Figure S6), which is in contrast with the parent complex.

The isolated photoproduct $\mathbf{A}^{2+}$ shows five bands at 250, 285, 380, 492, and 575 nm in methanol (Figure 3 and Figure S7 (left)) and shows a quasi-reversible oxidation at 0.95 V vs Ag/AgCl (Figure 3). The full chemical reversibility of the oxidation was confirmed by UV−vis absorption spectroelectrochemistry with a full loss and recovery of visible absorbance with each cycle between 0.0 and 1.2 V. The visible absorption bands are similar to those reported[17,18] for the iron(II) complex of a bis-tridentate bidentate imine-based iron(II) complex ($\mathbf{B}^{2+}$, see Scheme S1 for details) and are distinct from that of $[(MeN4Py)Fe^{II}{-}OCH_3]$.[19] The spectrum is identical in methanol and in acetonitrile, indicating that the solvent is not coordinated in $\mathbf{A}^{2+}$. $\mathbf{A}^{2+}$ shows no signals in its EPR (X-band) spectrum at 77 K (Figure S7 (right)) and shows a ^{1}H NMR spectrum (*vide infra*) that is consistent with the assignment of $\mathbf{A}^{2+}$ as a low-spin (diamagnetic) mononuclear Fe(II) complex.

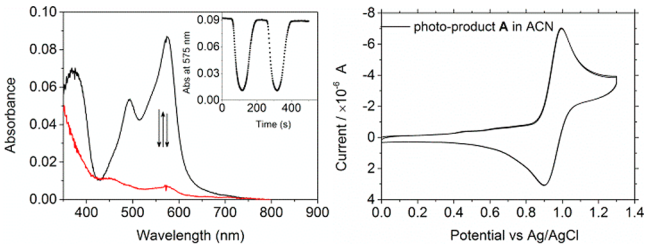

Figure 3. (Left) UV−vis absorption spectrum of $\mathbf{A}^{2+}$ before and after oxidation at 1.2 V (inset: absorbance at 575 nm during cyclic voltammetry in an OTTLE cell). (Right) Corresponding cyclic voltammetry of $\mathbf{A}^{2+}$ in acetonitrile (0.1 M $TBAPF_6$).

The positive mode ESI/MS spectra of $\mathbf{A}^{2+}$ in methanol (Figure S8) and acetonitrile show the same base peak at 316.3 m/z and a singly charged peak at 731.4 m/z corresponding to $\mathbf{A}^{2+}$ and $[\mathbf{A}(ClO_4)]^+$, respectively. The ions are consistent with the complex $[L_2Fe(II)]^{2+}$, in which L is the MeN4Py ligand which has undergone a loss of one "pyridine-CH_2" moiety. This assignment is consistent with the spectral similarity of complex $\mathbf{A}^{2+}$ and pyridyl-imine-based complexes (Scheme S1 and Figure S9) reported by Stefano and co-workers.[17,18]

The presence of an imine bond in the ligand was confirmed by comparison of the non-resonant Raman and FTIR spectra of $\mathbf{A}^{2+}$ with those of $[(MeN4Py)Fe^{II}(CH_3CN)]^{2+}$ (**3**). The Raman spectrum of photoproduct $\mathbf{A}^{2+}$ in the solid state shows substantially modified ligand-based vibrational modes (1200–1600 cm^{-1}) compared to those of **3**. The band at 2270 cm^{-1}, a coordinated acetonitrile, is absent, and several intense bands at 1221, 1468, and 1551 cm^{-1} appear in the spectrum of $\mathbf{A}^{2+}$ that are absent in the spectrum of **3** (Figure 4). The FTIR spectrum of $\mathbf{A}^{2+}$ reveals the presence of the same counterion as that in **3** (perchlorate $\nu_{stretch}$ (s) = 1087 cm^{-1}), as well as additional bands at 1217, 1245, 1353, 1542, and 1582 cm^{-1}.

The formation of the 2:1 complex of $\mathbf{A}^{2+}$ implies that 50% of the iron is present as a second complex. Furthermore, the pyridyl-CH_2 moiety lost in the formation of L should be accounted for. FTIR analysis for the light yellow precipitate formed during the conversion of **1** to $\mathbf{A}^{2+}$ shows strong bands at 841, 1284, and 1616 cm^{-1}. The spectrum resembles those of iron(III) bis-picolinates, such as $[Fe^{III}{}_2(\mu\text{-}OMe)_2(Pic)_4]$ (PicH = 2-picolinic acid) which is formed upon mixing iron(III) salts and picolinic acid in methanol,[21] but with minor differences in band positions (of the carboxylato modes, Figure S10)[20] and is consistent with the absence of significant ESI/MS signals (as the complex is neutral) and EPR (X-band) signals at 77 K.

The ^{1}H NMR spectrum of $\mathbf{A}^{2+}$ in acetonitrile-d_3 shows signals of a diamagnetic species that has a pronounced

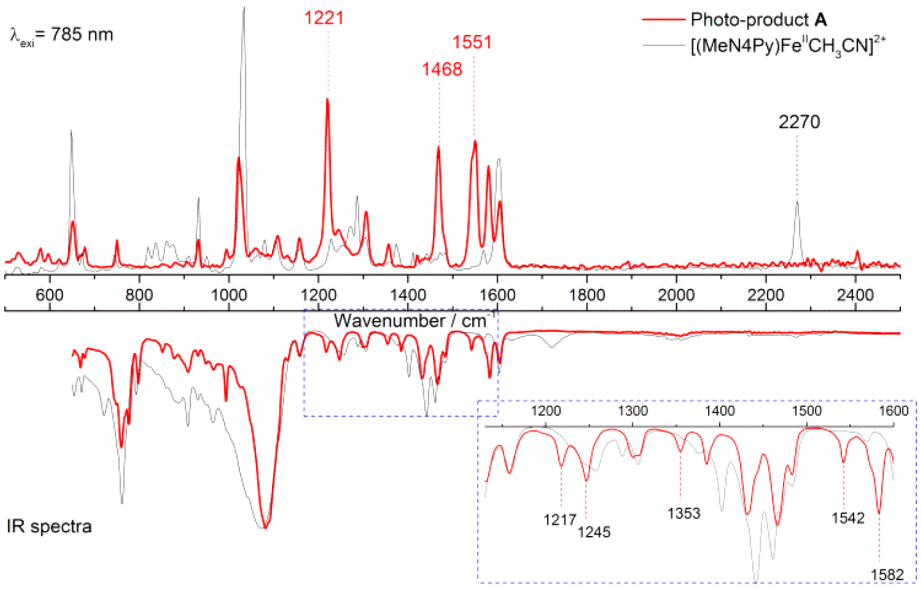

Figure 4. Raman (top) and FTIR (bottom) spectra of photoproduct $\mathbf{A}^{2+}$ that are compared with those of $[(MeN4Py)Fe^{II}CH_3CN](ClO_4)_2$ (**3**). Inset: expansion of the region between 1130 and 1600 cm^{-1}.

DOI: 10.1021/acs.inorgchem.8b00187
Inorg. Chem. 2018, 57, 4510−4515

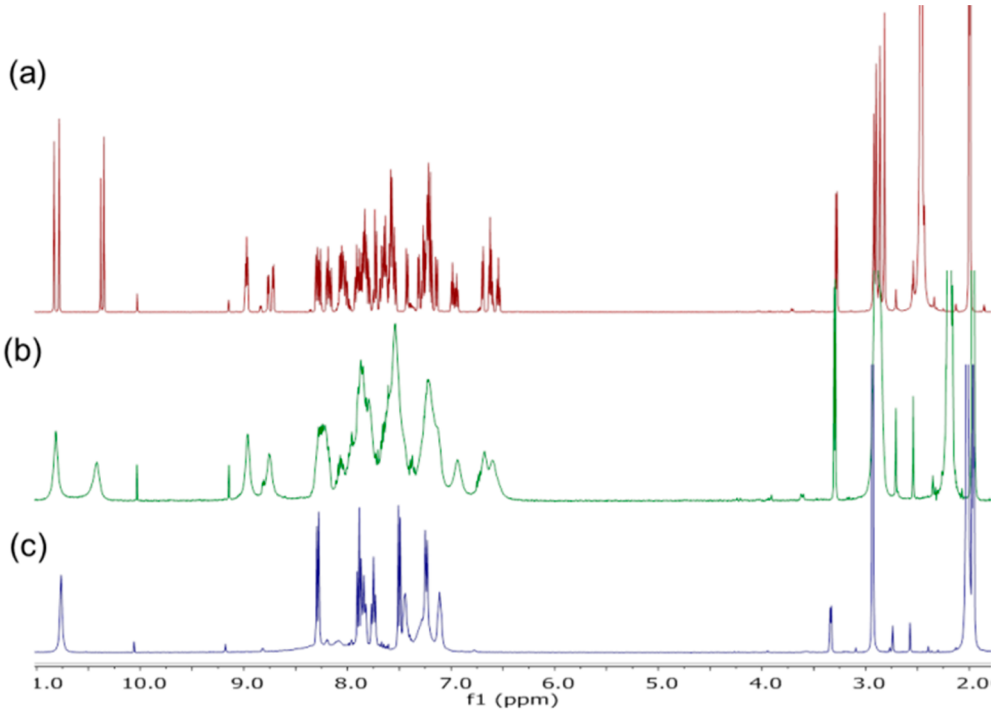

Figure 5. ^{1}H NMR spectra of photoproduct $\mathbf{A}^{2+}$ in CD_3CN at (a) −30 °C, (b) 25 °C, and (c) 75 °C.

temperature dependence (Figure 5). At −30 °C, the spectrum indicates the presence of several species (isomers). At higher temperatures, rapid interconversion (with respect to the ^{1}H NMR time scale) is observed, leading to a substantial simplification of the spectrum. Two-dimensional (2D) NMR experiments (HSQC, HMBC, COSY, and NOESY) were conducted at −30 °C and at 75 °C to gain insight into the conformational chemistry and isomerization of $\mathbf{A}^{2+}$. At 75 °C, only one set of signals, consistent with C_2 symmetry, is observed. The signals at 10.76 and 2.39 ppm are assigned to imine and methyl protons, respectively (Figures S11−S17).[22] Twelve pyridyl signals are expected in the aromatic region; however, two are absent, due to extensive broadening. At 25 °C two sets of signals of distinct conformers are observed, which confirms that the exchange between isomers is slow with respect to the ^{1}H NMR time scale. At −30 °C (Figures S18−S26), the integration is consistent with the presence of four sets of signals, each of which has C_2 symmetry. Two sets of four singlet signals at δ 10.85, 10.82, 10.44, and 10.40 ppm (with a ratio of 1:1.2:0.8:1) and 2.95, 2.91, 2.88, and 2.84 ppm (with a ratio of 0.8:1:1:1.2) are assigned to imine and methyl protons, respectively.[22] The 2D NOESY NMR spectra confirm exchange among the four conformers affecting the imine, methyl, and several of the pyridine protons (see the Supporting Information for details). The exchange pathways are proposed in Scheme 2.

On the basis of the experimental data, the proposed structure of $\mathbf{A}^{2+}$ was explored with the density functional theory (DFT) at the S12g level of theory; in particular, the relative stabilities, geometries, and electronic structure of conformers and diastereoisomers of the proposed bidentate imine-based Fe(II) complex $\mathbf{A}^{2+}$ were calculated. Stereochemical consideration of complex $\mathbf{A}^{2+}$ must take into account the two stereogenic centers and, hence, seven distinct isomers (diastereoisomers and conformers, Scheme S2). DFT calculations reveal that the four lowest-energy isomers are similar in energy (Table S1) and that it is reasonable to assume that the macroscopic properties

Scheme 2. Proposed Exchange Pathways for $\mathbf{A}^{2+}$ in Acetonitrile

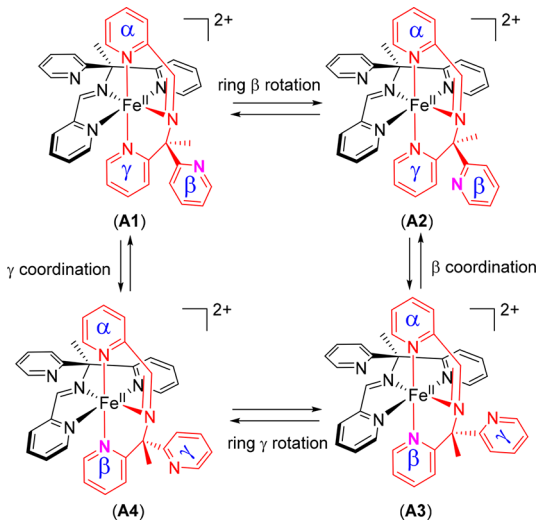

are manifestations of the properties of a mixture of isomers and not a single thermodynamically stable isomer. Separate optimization of the three possible spin states (low, intermediate, and high) indicates clearly that the low-spin S = 0 spin state is in all cases the spin ground state, with the other spin states around 20 kcal mol^{-1} higher in energy (Table S2), consistent with the fully diamagnetic character of the species, cf. ^{1}H NMR spectroscopy, and confirming that the temperature dependence is due to isomer interconversion and not paramagnetism.

Although both O_2 and a base are required for the formation of $\mathbf{A}^{2+}$, the mechanism by which the ligand is oxidized to lose a pyridyl-CH_2 moiety and forms an imine is less apparent. The requirement for O_2 to be present implies the formation of a reactive oxygen species, such as Fe(IV)═O, hydroxyl radical,

DOI: 10.1021/acs.inorgchem.8b00187
Inorg. Chem. 2018, 57, 4510−4515

superoxide, singlet oxygen (see SI), etc., that can engage in hydrogen atom abstraction (HAT) at the benzylic C−H of the MeN4Py ligand. However, the involvement of singlet oxygen and superoxide can be excluded, as neither results in the formation of photoproduct $\mathbf{A}^{2+}$ (see SI for details, Figures S27 and S28). Furthermore, the Fe(II) complex bearing the same ligand **1a** is not converted directly to $\mathbf{A}^{2+}$ (Figure S29 and Scheme S3). Irradiation of the structurally analogous (N4Py) complex $[(N4Py)Fe(III)\text{-}OCH_3]^{2+}$ (**2**) in air-equilibrated methanol with Et_3N results in a mixture of Fe(II) complexes with an intact ligand (<20%) and ill-defined ligand degradation products; no similar imine-based ligand complex "$\mathbf{A}^{2+}$" was observed (Figure S30).

Amine-based ligands are typically good donor ligands, and under irradiation ligand to metal charge transfer from the amine moiety to an iron(III) center is expected, yielding a transient aminium radical cation. The charge transfer lowers the bond dissociation energy of the C−H bonds at the amine α-positions[23] and facilities deprotonation and charge transfer to form a radical at the first methylene position. Such species are known to couple readily with O_2 to form an alkyl superoxide radical.[24] Hydrogen atom abstraction from a neighboring methylene position induces C−N bond cleavage and finally formation of an imine. O_2 plays an essential role in this mechanism; however, deprotonation is rate limiting, and irradiation serves to make the benzylic C−H bonds more acidic, accelerating the overall process (Scheme 3).

Scheme 3. Proposed Mechanism for Photoreduction and Degradation of 1[a]

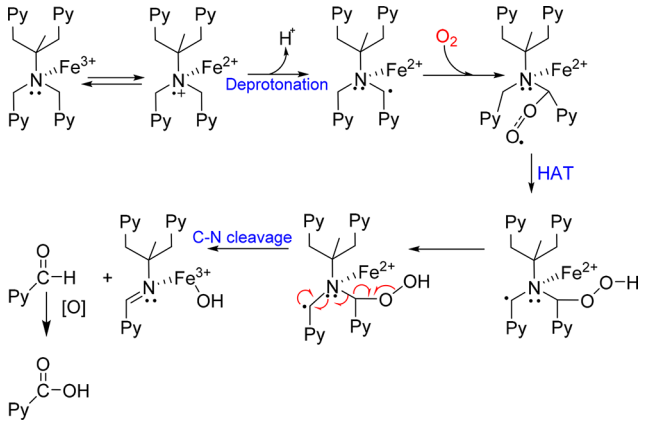

[a]Photoreduction and degradation of **1** is tentatively proposed to proceed through deprotonation at a pyridylic position followed by reaction of the alkyl radical with O_2 and intamolecular HAT. O−O bond homolysis and C−N bond cleavage lead to the formation of an imine unit, and subsequent ligand scrambling leads to the formation of $\mathbf{A}^{2+}$ and Fe(III) bispicolinato complexes.

Oxidative cleavage of a C−N bond was reported for the cobalt(II) complex of *N*-methyl-*N*,*N*′-bis(2-pyridylmethyl)-ethylenediamine-*N*′-acetate (mebpena-), in which Co(III)-superoxide intermediates were proposed to react with methylene units with HAT as an initial step toward C−N cleavage.[25] The first iron(III) assisted oxidative cleavage of a C−N bond was reported by Morgenstern-Badarau following a similar mechanism.[26] In both cases, the products of the oxidative C−N cleavage of the tertiary amine ligand were secondary amines. In the present study, to the best of our knowledge, this is the first example of oxidative cleavage of a C−N bond leading to the formation of an imine ligand .

CONCLUSIONS

In summary, we report the highly selective oxidative ligand degradation in a non-heme iron(III) complex to form a well-defined imine-based 2:1 iron(II) complex under basic conditions with O_2 as the terminal oxidant. The reaction is accelerated dramatically by irradiation with near-UV and visible light; however, for both thermally and photochemically driven reactions, the initial step is assigned to deprotonation to form an alkylamine radical that subsequently undergoes reaction with O_2 instead of the formation of other reactive oxygen species, such as superoxides, hydroxyl radicals, or H_2O_2. The ligand degradation pathway holds implications for the design of ligands for oxidation catalysts based on the pyridyl-methyl-amine motif, where degradation is expected to be due to attack of reactive oxygen species and high-valent iron oxido complexes on the ligand. Here, we show that base catalyzed pathways are important also and that the observations may help rationalize in part the increased efficiency of such catalysts under acid conditions.

EXPERIMENTAL SECTION

Synthesis of complexes **1**−**3**, as well as the irradiation details, are described in the Supporting Information.

Physical Methods. UV−vis absorption spectra were recorded with a Specord 600 (AnalytiJena) spectrometer in a 1 cm path length quartz cuvette. ESI mass spectra of the complexes were recorded on a Triple Quadrupole LC/MS/MS mass spectrometer (API 3000, PerkinElmer Sciex Instruments). ^{1}H NMR spectra were recorded on a Varian Mercury 400 or Unity 500 MHz spectrometer. Chemical shifts are denoted relative to the residual solvent peak (^{1}H NMR spectra, CD_3CN, 1.94 ppm). Electrochemical measurements were carried out by a model CHI760B electrochemical workstation (CH Instruments) in acetonitrile using 0.1 M TBAPF6, 3 mm diameter Teflon-shrouded glassy carbon, a Pt wire, and an SCE electrode, the latter three of which were used as the working, counter, and reference electrodes, respectively. EPR (X-band, 9.46 GHz) spectra were recorded on a Bruker ECS106 spectrometer in liquid nitrogen (77 K). Samples (0.4 mL), monitored by UV−vis absorption spectroscopy, were flash frozen in liquid nitrogen. FTIR spectra were recorded using a UATR (ZnSe) accessory with a PerkinElmer Spectrum400, equipped with a liquid nitrogen cooled MCT detector. Raman spectra were recorded at λ_{exc} = 785 nm using a PerkinElmer Raman Station at room temperature. Raman spectra at 532 nm (300 mW at source, Cobolt Lasers) were obtained in a 180° backscattering arrangement, with Raman scattering collected, collimated, and subsequently refocused via a pair of 2.5 cm diameter plano-convex lenses (f = 7.5 and 10 cm) into a Sharmrock300i spectrograph (Andor Technology) with a 1200 L/mm grating blazed at 500 nm, and were acquired with a Newton DU970N−BV or a iDus-420-BUE2 CCD camera (Andor Technology). The slit width was set at 50 μm, and an appropriate long pass filter was placed in front of the focusing lens.

ASSOCIATED CONTENT

Supporting Information

The Supporting Information is available free of charge on the ACS Publications website at DOI: 10.1021/acs.inorgchem.8b00187.

Experimental details and additional figures and schemes (including an NMR analysis and computational sections) (PDF)

DOI: 10.1021/acs.inorgchem.8b00187
Inorg. Chem. 2018, 57, 4510−4515

AUTHOR INFORMATION

Corresponding Authors

*E-mail: gmaja@chem.bg.ac.rs.
*E-mail: w.r.browne@rug.nl.

ORCID

Maja Gruden: 0000-0002-0746-5754
Wesley R. Browne: 0000-0001-5063-6961

Notes

The authors declare no competing financial interest.

ACKNOWLEDGMENTS

The European Research Council (ERC 279549 to W.R.B.), the Serbian Ministry of Science (OI172035 to M.G.), the Chinese Scholarship Council (CSC to J.C.), and The Netherlands Ministry of Education, Culture, and Science (Gravity program 024.001.035 to W.R.B.) are acknowledged for their financial support. This work was performed in the framework of COST Action CM1305 (STSM 38503 and 39551) "Explicit Control Over Spin-states in Technology and Biochemistry (ECOST-Bio)".

REFERENCES

(1) Oloo, W. N.; Que, L., Jr Bioinspired Nonheme Iron Catalysts for C-H and C = C Bond Oxidation: Insights into the Nature of the Metal-Based Oxidants. *Acc. Chem. Res.* **2015**, *48*, 2612−2621.

(2) Rohde, J.-U.; In, J.-H.; Lim, M. H.; Brennessel, W. W.; Bukowski, M. R.; Stubna, A.; Münck, E.; Nam, W.; Que, L., Jr Crystallographic and Spectroscopic Characterization of a Nonheme Fe(IV)═O Complex. *Science* **2003**, *299*, 1037−1039.

(3) Lim, M. H.; Rohde, J.-U.; Stubna, A.; Bukowski, M. R.; Costas, M.; Ho, R. Y. N.; Münck, E.; Nam, W.; Que, L., Jr An FeIVO Complex of a Tetradentate Tripodal Nonheme Ligand. *Proc. Natl. Acad. Sci. U. S. A.* **2003**, *100*, 3665−3670.

(4) Kaizer, J.; Klinker, E. J.; Oh, N. Y.; Rohde, J.-U.; Song, W. J.; Stubna, A.; Kim, J.; Münck, E.; Nam, W.; Que, L., Jr Nonheme $Fe^{IV}O$ Complexes That Can Oxidize the C−H Bonds of Cyclohexane at Room Temperature. *J. Am. Chem. Soc.* **2004**, *126*, 472−473.

(5) Roelfes, G.; Lubben, M.; Hage, R.; Que, L., Jr.; Feringa, B. L. Catalytic Oxidation with a Non-Heme Iron Complex That Generates a Low-Spin $Fe^{III}OOH$ Intermediate. *Chem. - Eur. J.* **2000**, *6*, 2152.

(6) Sastri, C. V.; Sook Seo, M.; Joo Park, M.; Mook Kim, K.; Nam, W. Formation, Stability, and Reactivity of a Mononuclear Nonheme oxoiron(IV) Complex in Aqueous Solution. *Chem. Commun.* **2005**, *2*, 1405−1407.

(7) England, J.; Guo, Y.; Farquhar, E. R.; Young, V. G., Jr.; Münck, E.; Que, L., Jr The Crystal Structure of a High-Spin oxoiron(IV) Complex and Characterization of Its Self-Decay Pathway. *J. Am. Chem. Soc.* **2010**, *132*, 8635−8644.

(8) Oh, N. Y.; Suh, Y.; Park, M. J.; Seo, M. S.; Kim, J.; Nam, W. Mechanistic Insight into Alcohol Oxidation by High-Valent Iron-Oxo Complexes of Heme and Nonheme Ligands. *Angew. Chem., Int. Ed.* **2005**, *44*, 4235−4239.

(9) Thibon, A.; Bartoli, J.-F.; Bourcier, S.; Banse, F. Mononuclear Iron Complexes Relevant to Nonheme Iron Oxygenases. Synthesis, Characterizations and Reactivity of Fe-Oxo and Fe-Peroxo Intermediates. *Dalton Trans.* **2009**, *43*, 9587.

(10) England, J.; Davies, C. R.; Banaru, M.; White, A. J. P.; Britovsek, G. J. P. Catalyst Stability Determines the Catalytic Activity of Non-Heme Iron Catalysts in the Oxidation of Alkanes. *Adv. Synth. Catal.* **2008**, *350*, 883−897.

(11) Grau, M.; Kyriacou, A.; Cabedo Martinez, F.; de Wispelaere, I. M.; White, A. J. P.; Britovsek, G. J. P. Unraveling the Origins of Catalyst Degradation in Non-Heme Iron-Based Alkane Oxidation. *Dalton Trans.* **2014**, *43*, 17108−17119.

(12) Company, A.; Sabenya, G.; González-Béjar, M.; Gómez, L.; Clémancey, M.; Blondin, G.; Jasniewski, A. J.; Puri, M.; Browne, W. R.; Latour, J.-M.; et al. Triggering the Generation of an Iron(IV)-Oxo Compound and Its Reactivity toward Sul Fi Des by Ru. *J. Am. Chem. Soc.* **2014**, *136*, 4624−4633.

(13) Kotani, H.; Suenobu, T.; Lee, Y.-M.; Nam, W.; Fukuzumi, S. Photocatalytic Generation of a Non-Heme Oxoiron(IV) Complex with Water as an Oxygen Source. *J. Am. Chem. Soc.* **2011**, *133*, 3249−3251.

(14) Chen, J.; Draksharapu, A.; Harvey, E.; Rasheed, W.; Que, L.; Browne, W. R. Direct Photochemical Activation of Non-Heme Fe(iv)[double Bond, Length as M-dash]O Complexes. *Chem. Commun.* **2017**, *53*, 12357−12360.

(15) Chen, J.; Stepanovic, S.; Draksharapu, A.; Gruden, M.; Browne, W. R. A Non-Heme Iron Photocatalyst for Light Driven Aerobic Oxidation of Methanol. *Angew. Chem., Int. Ed.* **2018**, *57*, 3207.

(16) Draksharapu, A.; Li, Q.; Roelfes, G.; Browne, W. R. Photo-Induced Oxidation of [FeII(N4Py)CH_3CN] and Related Complexes. *Dalton Trans.* **2012**, *41*, 13180−13190.

(17) Olivo, G.; Nardi, M.; Vìdal, D.; Barbieri, A.; Lapi, A.; Gómez, L.; Lanzalunga, O.; Costas, M.; Di Stefano, S. C-H Bond Oxidation Catalyzed by an Imine-Based Iron Complex: A Mechanistic Insight. *Inorg. Chem.* **2015**, *54*, 10141−10152.

(18) Olivo, G.; Arancio, G.; Mandolini, L.; Lanzalunga, O.; Di Stefano, S. Hydrocarbon Oxidation Catalyzed by a Cheap Nonheme Imine-Based Iron(II) Complex. *Catal. Sci. Technol.* **2014**, *4*, 2900−2903.

(19) Draksharapu, A.; Li, Q.; Logtenberg, H.; van den Berg, T. A.; Meetsma, A.; Killeen, J. S.; Feringa, B. L.; Hage, R.; Roelfes, G.; Browne, W. R. Ligand Exchange and Spin State Equilibria of FeII(N4Py) and Related Complexes in Aqueous Media. *Inorg. Chem.* **2012**, *51*, 900−913.

(20) Kalinowska, M.; Borawska, M.; Świsłocka, R.; Piekut, J.; Lewandowski, W. Spectroscopic (IR, Raman, UV, ^1H and ^{13}C NMR) and Microbiological Studies of Fe(III), Ni(II), Cu(II), Zn(II) and Ag(I) Picolinates. *J. Mol. Struct.* **2007**, *834-836*, 419.

(21) Kiani, S.; Tapper, A.; Staples, R. J.; Stavropoulos, P. Functional Aspects of Gif-Type Oxidation of Hydrocarbons Mediated by Iron Picolinate H_2O_2-Dependent Systems: Evidence for the Generation of Carbon- and Oxygen-Centered Radicals. *J. Am. Chem. Soc.* **2000**, *122*, 7503−7517.

(22) Chavez-Gil, T. E.; Yasaka, M.; Senokuchi, T.; Sumimoto, M.; Kurosaki, H.; Goto, M. Successive Intramolecular Transiminations in an Iron (II) Complex with Chiral Tridentate Ligands. *Chem. Commun.* **2001**, 2388−2389.

(23) Dinnocenzo, J. P.; Banach, T. E. Deprotonation of Tertiary Amine Cation Radicals. A Direct Experimental Approach. *J. Am. Chem. Soc.* **1989**, *111*, 8646−8653.

(24) Anjana, S.; Donring, S.; Sanjib, P.; Varghese, B.; Murthy, N. N. Controlling the Oxidation of Bis-Tridentate Cobalt(II) Complexes Having bis(2-Pyridylalkyl)amines: Ligand vs. Metal Oxidation. *Dalton Trans.* **2017**, *46*, 10830−10836.

(25) Vad, M. S.; Nielsen, A.; Lennartson, A.; Bond, A. D.; McGrady, J. E.; McKenzie, C. J. Switching on Oxygen Activation by Cobalt Complexes of Pentadentate Ligands. *Dalton Trans.* **2011**, *40*, 10698−10707.

(26) Rodriguez, M.-C.; Lambert, F.; Morgenstern-Badarau, I.; Cesario, M.; Guilhem, J.; Keita, B.; Nadjo, L. Selective Metal-Assisted Oxidative Cleavage of a C−N Bond: Synthesis and Characterization of the Mononuclear Iron(III) [Fe(BPG)Cl_2] Complex and Its Two [Fe(BPA)Cl_3] and [Fe(BPE)Cl_3] Derivatives. *Inorg. Chem.* **1997**, *36*, 3525−3531.

DOI: 10.1021/acs.inorgchem.8b00187
Inorg. Chem. 2018, 57, 4510−4515